An Exponential Luminous Efficiency Model for Hypervelocity Impact into Regolith

W. R. Swift • D. E. Moser • R. M. Suggs • W. J. Cooke

Abstract The flash of thermal radiation produced as part of the impact-crater forming process can be used to determine the energy of the impact if the luminous efficiency is known. From this energy the mass and, ultimately, the mass flux of similar impactors can be deduced. The luminous efficiency, η, is a unique function of velocity with an extremely large variation in the laboratory range of under 6 km/s but a necessarily small variation with velocity in the meteoric range of 20 to 70 km/s. Impacts into granular or powdery regolith, such as that on the moon, differ from impacts into solid materials in that the energy is deposited via a serial impact process which affects the rate of deposition of internal (thermal) energy. An exponential model of the process is developed which differs from the usual polynomial models of crater formation. The model is valid for the early time portion of the process and focuses on the deposition of internal energy into the regolith. The model is successfully compared with experimental luminous efficiency data from both laboratory impacts and from lunar impact observations. Further work is proposed to clarify the effects of mass and density upon the luminous efficiency scaling factors.

Keywords hypervelocity impact · impact flash · luminous efficiency · lunar impact · meteoroid

1 Introduction

The impact of meteoroids on the lunar surface is accompanied by a brief flash of light, detectable with small telescopes from the ground, Figure 1. These impact flashes have been successfully observed on the Moon by Earth-based telescopes during several showers (e.g. Dunham et al., 2000; Ortiz et al., 2000; Cudnick et al., 2002; Ortiz et al., 2002; Yanagisawa & Kisaichi, 2002; Cooke et al., 2006; Yanagisawa et al., 2006, Cooke et al., 2007; Suggs et al., 2008a,b; Yanagisawa et al., 2008) and for sporadic meteoroids by a campaign conducted by the NASA Marshall Space Flight Center (MSFC) since early 2006. Although the initial shock wave from a hypervelocity impact produces a significant high temperature plasma and blackbody flash lasting on the order of microseconds as the shock wave passes through the material this is generally buried below the regolith surface and not readily observable, Figure 2 lower (Ernst and Schultz, 2007). Also obscured and/or quenched by the regolith is the plasma and vapor plume observed from impacts into solid surfaces, Figure 2 upper, as modeled in early lunar impact models (Melosh et al., 1993; Nemtchinov et al., 1998). What is observed at video rates by terrestrial telescopes is the secondary blackbody radiation from the cooling hot debris thrown upwards in

W. R. Swift (✉)
Jacobs ESTS Group/Raytheon, NASA/Marshall Space Flight Center, Huntsville, AL, 35812 USA. E-mail: wesley.r.swift@nasa.gov

D. E. Moser
MITS/Dynetics, NASA/Marshall Space Flight Center, Huntsville, AL, 35812 USA

R. M. Suggs • W. J. Cooke
Meteoroid Environment Office, NASA/Marshall Space Flight Center, Huntsville, AL, 35812 USA

the initial moments of crater formation. Since the optical energy of such flashes can be readily measured telescopically, it is highly desirable to be able to estimate the energy of the meteoroid impact given the luminous efficiency η of the event. The concern then is how the luminous efficiency scales with the velocity, mass, and density of the impactor.

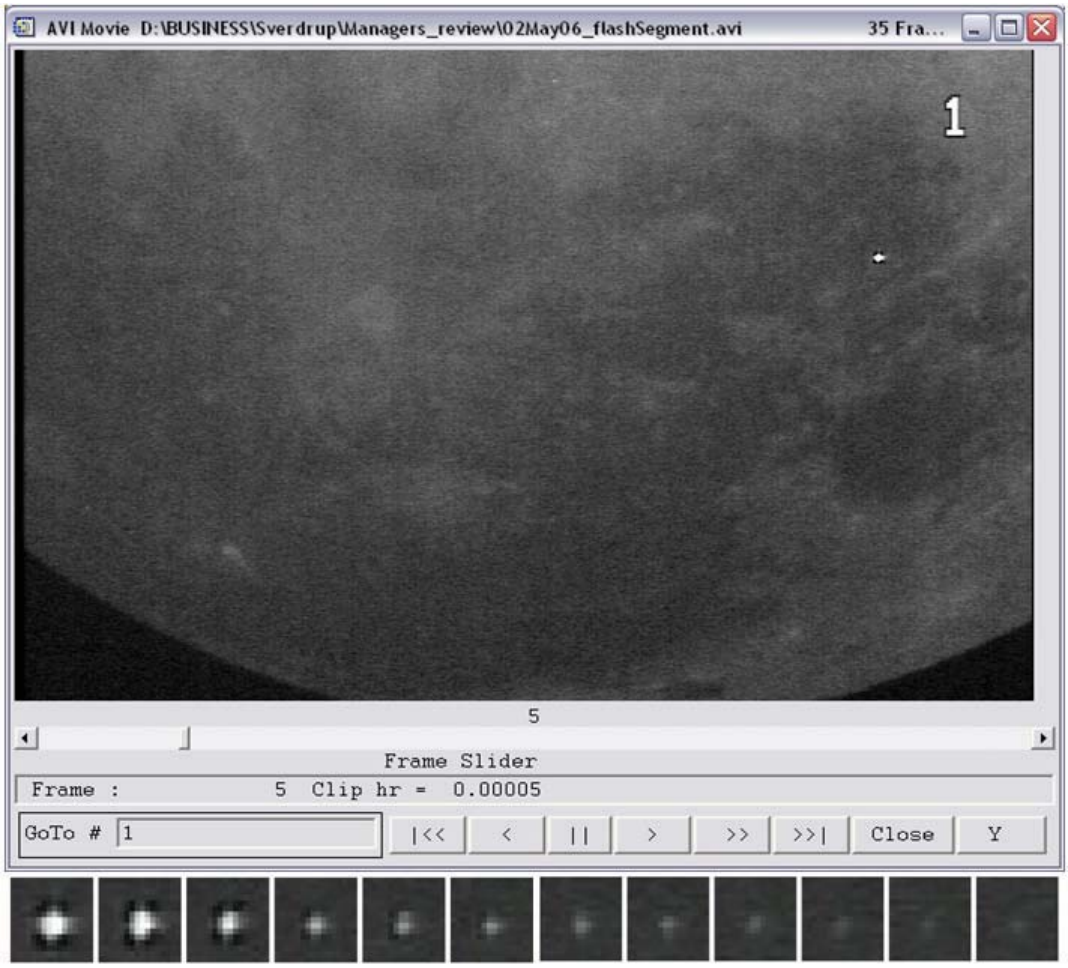

Figure 1. Lunar impact as seen on May 2, 2006 with a 254mm aperture telescope at 30 frames/second. The lower sequence shows a magnified view of the flash decay versus frame. This impact is one of the brighter impacts observed to date.

Similarly, in light gas gun experiments into pumice and lunar simulant, Figure 2, there is often a very brief (microsecond) high temperature spike recordable by high speed photodiodes (Ernst and Schultz, 2004, 2007). This early-time spike is followed over the next tenth(s) of a second by a slowly decaying secondary production of light from the hot ejecta. Moderately fast ejecta particle trails are quite evident in video rate (1/30 second) images of gas gun tests as is the cooling of the ejecta from frame to frame. Although the first video field after impact is usually the brightest, localized initial shock heating is not readily apparent in the hot ejecta dominated image. High speed camera images of lab tests (not shown) also show the primary source of illumination to be hot ejecta moving up, away from the impact rather than primary emissions from the shock wave propagating down into the target. Due to the much longer time period of these secondary emissions, their total output is significantly larger than the

brief but intense shock and plasma emissions. This is especially true since most of the prompt emissions are hidden beneath the impactor and the particulate target surface.

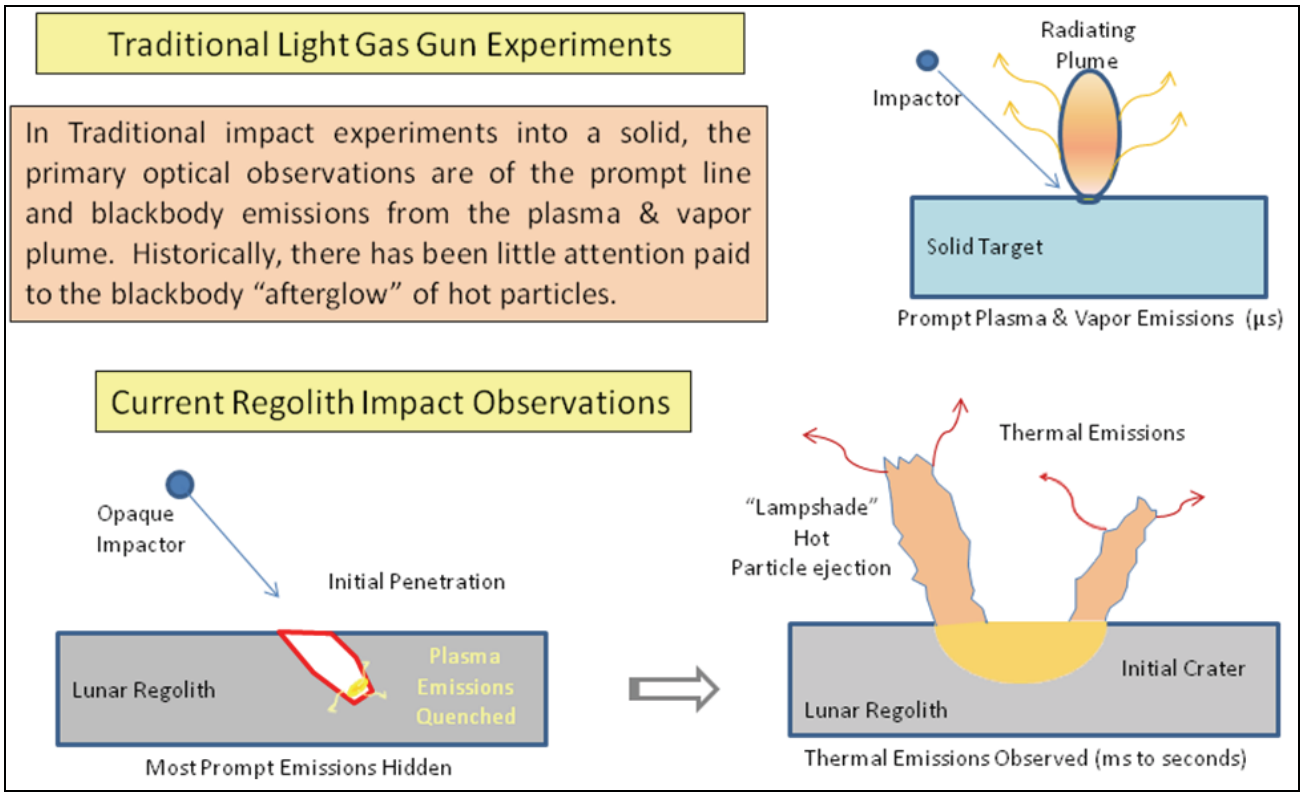

Figure 2. Traditional hypervelocity impact observations compared with impact into regolith. The emissions are thermal in nature and much longer lasting.

A series of light gas gun experiments were conducted at the Ames Vertical Gun Range (AVGR) in which a Pyrex® glass bead was shot into JSC-1a lunar regolith simulant (McKay et al., 1997; Zeng et al., 2010) at various angles and velocities. It was a relatively simple matter to calculate the luminous efficiency of light gas gun experiments since the mass, material properties, and velocity of the impactor were precisely known and the flash intensity readily measured. A problem arose when one attempted to correlate this luminous efficiency with velocity over the small range of velocities (< 7 km/s) available to the technique. The increase of luminous efficiency with velocity between 2 km/s and 6 km/s was so steep that polynomial fits extrapolate to unrealistic ($\eta > 1$) values well before the usual meteoroid velocities, V_m, of some tens of km/s. Furthermore, if curves analogous to conventional impact crater dimension scaling with exponents of V^1 to V^2 (Holsapple, 1993) are plotted through the luminous efficiency versus velocity data (almost vertical) they appear orthogonal (almost horizontal) to the data from these experiments. This implies the existence of additional phenomena that scales quite differently from conventional impact crater dimension scaling.

In order to determine an appropriate model of impact luminous efficiency versus impact velocity, it is useful to briefly examine the internal energy produced by the initial impact shock wave itself and early post shock conditions. One can then relate these conditions to the special case of the luminous efficiency of an impact into lunar regolith to obtain evidence leading to an appropriate model. Finally, this model will be compared to knowledge of the luminous efficiency from both light gas gun experiments and the growing database of lunar impact measurements.

2 Lunar Impact Luminous Efficiency

It is useful to estimate the kinetic energy of an impactor on the moon's surface from the total optical energy detected by a camera, E_λ, using a ratio known as the luminous efficiency, η_λ defined as:

$$\eta_\lambda \equiv E_\lambda / KE_{impactor} \quad (1)$$

where E_λ is defined as that energy at the source which is radiated into all space (4π steradians) as measured by that proportion received in the camera aperture and $KE_{impactor}$ is the kinetic energy of the impactor. Previous work has assumed surface radiation into 2π steradians (Swift et al. 2008) or radiation into 3π steradians (Belio Rubio et al. 2000). The geometric projection removes the effect of telescope aperture from the measurements leaving bandpass considerations unresolved. Initial assumptions that the radiation was from the early crater surface and thus into 2π steradians were abandoned when it was realized that the primary radiation was from free particles above the surface. E_λ is instrument specific, leading to the camera optical ratio, $O_c \equiv E_\lambda / E_t$, with an alternate definition of luminous efficiency, η_t or total luminous efficiency, based on total radiant energy, E_t

$$\eta_t \equiv E_t / KE_{impactor} = \sum_i m_i E_i' / KE_{impactor} \quad (2)$$

where the summation is over i particles of mass m_i and specific energy E'_i. Note that O_c is less than unity and is a function of the camera spectral response convolved with the declining blackbody emissions over the time of the observation. Improvements in the determination of O_c and the variation from camera to camera are underway but the distinctions between E_λ and E_t, are poorly defined. Note that, unlike the rate of thermal emissions, which is fourth power in temperature, E_t, is the integral over time and is almost linear in temperature since the thermal specific energy for each particle is the specific heat capacity, Cp, times the temperature change, ΔT, during emission, $E'_i = Cp\Delta T_i$. Unless otherwise defined, whenever η is mentioned it is usually safe to assume that η_λ is implied for the purpose of this paper.

NASA's Marshall Space Flight Center has been consistently monitoring the Moon for impact flashes produced by meteoroids striking the lunar surface since early 2006 (Cooke et al 2006). The 2006 Geminids, 2007 Lyrids, and 2008 Taurids, Table 1 below, produced a small but sufficient, sample of lunar impact flashes with which to perform a luminous efficiency analysis like that outlined in Bellot Rubio et al. (2000b). The analysis technique, discussed in detail by Moser et al. (2010), involves 'backing out' the luminous efficiency by relating the number of impacts expected on the Moon as a function of energy to the time integral of the flux of meteors of known size and the lunar area perpendicular to the shower radiant of known mass index, S. The resulting luminous efficiencies for the cameras used for the observations are shown in Table 1 with the published results of Bellot Rubio et al. (2000b) for the 1999 Leonids. Although their results are for a less sensitive camera and are based on the assumption of radiation into 3π steradians rather than 4π as assumed here, the results are consistent with the current determinations. Also shown are the results of hydrocode modeling of the 1999 Leonids by Artemieva et al. (2000, 2001). Although the agreement of this hydrocode model to the other results is entirely fortuitous, it is shown here for reference purposes. Expected errors are less than ± 20% for the camera dependant luminous efficiency. Note the almost constant luminous efficiency, η_λ, over these velocities.

Table 1. Luminous Efficiency from Lunar Impact Observations (Moser et al., 2010).

Shower	# Flashes	Obs. Time (hr)	V (km/s)	S (mass index)	η_λ
2008 Taurids	12	7.93	27	1.8	1.6×10^{-3}
2006 Geminids	12	2.18	35	1.9	1.2×10^{-3}
2007 Lyrids	12	10.22	49	1.7	1.4×10^{-3}
1999 Leonids*	5	1.5	71	2	2×10^{-3}*
1999 Leonids**	N/A	(model)	71	N/A	$1\times10^{-3}/2\times10^{-3}$

* Bellot Rubio et al. (2000) results for a different camera and slightly different geometry.
** Artemieva et al. (2000, 2001) hydrocode model results for densities 0.1 / 1.0 g/cm^3.

3 Light Gas Gun Camera Angle, Impact Angle and Velocity Experiments

A series of hypervelocity impacts into JSC-1a lunar regolith simulant at various angles and velocities were observed with the same video cameras used for lunar impact monitoring (Suggs et al. 2008b). Multiple cameras at three view angles were used in staring mode at the video rate of 29.97 frames per second. Their field of view, Figure 3 left, comprised the complete impact zone and the lenses were fitted with calibrated neutral density filters to obtain correct exposures. This contrasts with traditional light gas gun observations as illustrated in Figure 2, particularly in the time scale here of hundreds of milliseconds as opposed to hundreds of microseconds or less. Due to the long exposure sequence and good near IR sensitivity of the cameras, the hot ejecta from these impacts forms a cooling curve lasting multiple frames very similar to the bulk of the signals observed in lunar meteoroid impacts.

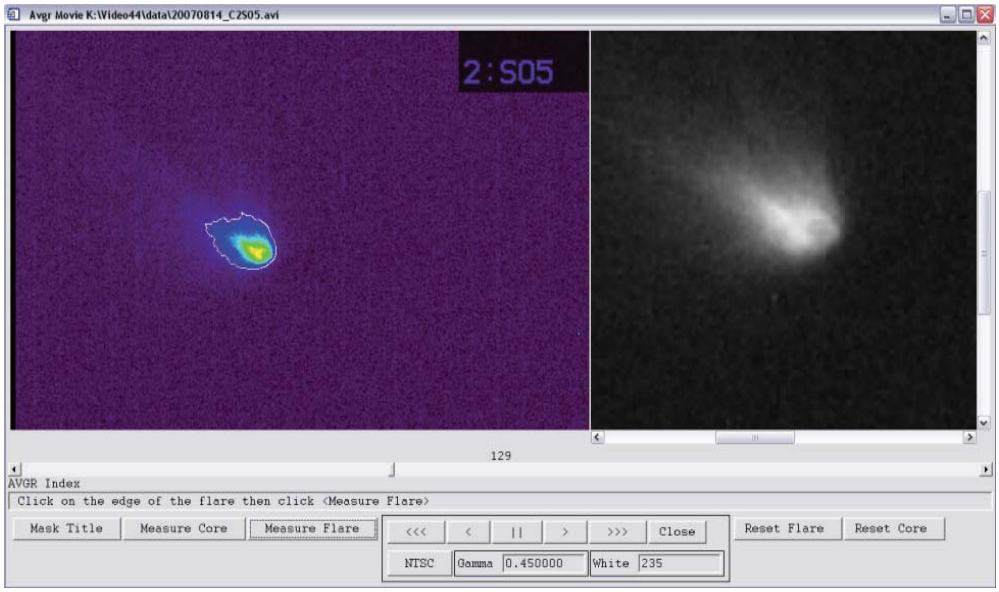

Figure 3. Software was written to semi-automatically determine the illuminated area and to compensate for background and video intensity scaling. The complete "encircled" image is in the false color image on the left while an enlarged view centered on the impact is to the right.

For these experiments, Pyrex® spheres 6.35mm in diameter and of mass 0.29 g were fired in vacuum at velocities from 2.4 km/s to 5.75 km/s at elevations of 15 to 90 degrees into a deep horizontal pan of JSC-1a lunar simulant. The cameras were mounted to observe at three angles: A) camera 2 with a 25mm lens used at f/10.84 was aimed near normal at 65 degrees elevation, 2.13m from impact, B)

camera 3 with a 25mm lens used at f/12.04 was aimed at 33 degrees elevation, 1.75m from the impact and C) camera 5 with a 17mm lens used at f/4.0 viewed horizontally 1.3m from the impact. Cameras 2 and 3 were StellacamEX video cameras set at the gain used for lunar meteor impact observations. For these observations the cameras were fitted with Andover precision neutral density filters from optical density (OD) from OD 1.02 to OD 3.77. These dark filters were chosen to keep the extremely bright signals from saturating the images. Camera 5 was a Watec model 902-H2 Ultimate with the same charge coupled device (CCD), gain, and filters as the others. A parallel set of cameras fitted with photographic grade neutral density filters had radiation leaks in the IR so the data was discarded. Laboratory and stellar calibrations were used to determine the electron gain of these cameras and the published quantum efficiency curve, *QE(λ)*, for the Sony ICX248AL CCD was used to evaluate spectral response. The *QE* was used to convert from photon counts, which these cameras measure, to detected energy in order to determine η. Software was written in the Interactive Data Language (IDL) computer language, Figure 3, to isolate the flash area in each image, compensate for NTSC-J video scaling, measure the intensity, subtract backgrounds, and calibrate the results. The total emission meaning that from all illuminated pixels for all illuminated frames is used to calculate η as shown in Figure 4.

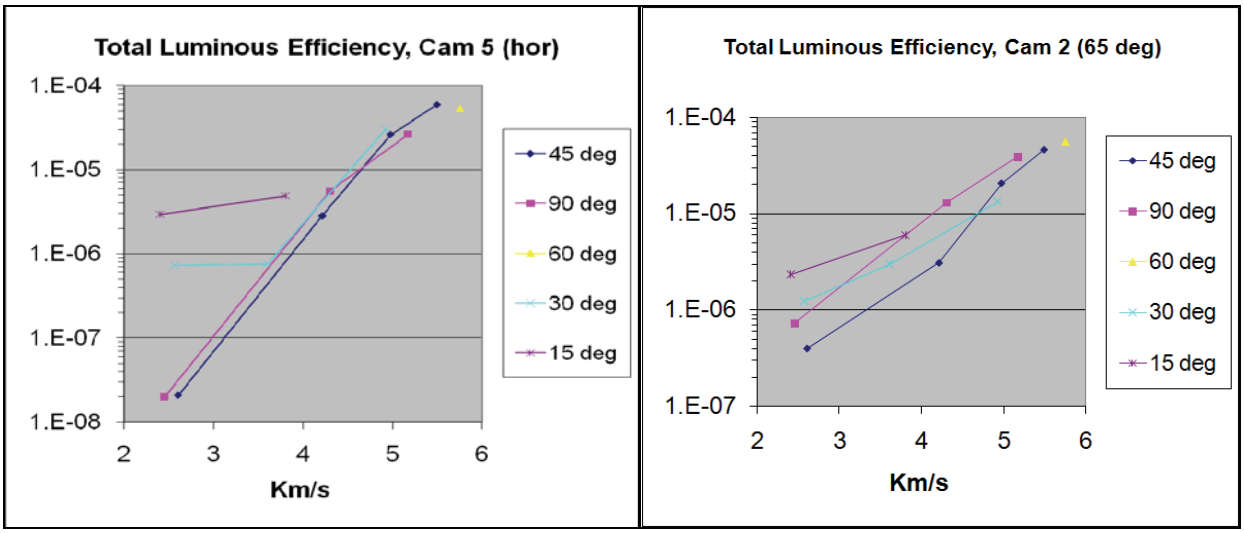

Figure 4. Total luminous efficiency of impacts of Pyrex into JAS-1 versus velocity and impact elevation. On the left is the horizontal view and on the right is the view from above. Note the convergence in both elevation and view angle near 5.5 km/s.

A brief examination of the variation of η with velocity and angle of impact in Figure 4, shows a convergence in both tangential (horizontal) and normal (overhead) views to very similar values at higher velocities for all angles of incidence. The low velocity enhancement of low angle impacts due to the "plowing up" of particles is evident as well as the negation of the effect at higher velocities. The low velocity, low angle of incidence η can be "compensated" to an equivalent η at normal incidence with a simple sine function of the impact angle that disappears above 4.4 km/s: , $\eta_c = \eta$*Sin(i)^(4.4-MIN(4.4,v))*. One can see the effect of incidence compensation in Figure 5 where the normal data is shown as blue diamonds and the compensated normal data with yellow triangles. This compensation makes comparison with meteoroid impacts more realistic. The independence of luminous efficiency with angle of incidence at high velocities was also noted by Artemieva et al. (2000) and Nemtchinov et

al. (1998). It is also a very convenient result for lunar impact observations since the impact angle is often unknown.

It is also desirable to correct for view angle, particularly since, due to gun emplacement, the normal view is not available. A useful viewing geometry, although inexact, is that of an oblate spheroid having a unit circle projection from above (normal) and an elliptical projection seen from any other angle. Development of this spheroid cross section model is straight forward. One lets the tangential view be approximated by a standard ellipse with unity half width a and half height b with area πab. The normal view is a circle with unit radius a and area πa^2 so that the tangential cross section ratio is b/a or just b. The height of the cross section of the spheroid viewed from angle θ is given by the radius in polar form of the ellipse where r, is given by $r^2 = a^2b^2 / (a^2 \sin^2\theta + b^2 \cos^2\theta)$. The area at view angle θ is πar so that the cross section ratio is simply r. Given experimental normal and tangential emission components at various velocities, their ratio can be used to determine the parameter, $b = 0.8V - 0.13$, a function of velocity which becomes unity (spherical) above 10.9 km/s. This has been used to correct the camera 2 data to the normal in Figure 5 prior to impact angle compensation. The primary lesson learned from this is that the surface intensity ellipse converges to a sphere and view angle effects are minimal for the higher velocities found in lunar meteoroid impacts: a very convenient result. Furthermore, it is the normal result from impact experiments that is to be compared with meteoroid impacts. A likely explanation is that at high impact velocities, most of each particle's emission is into free space significantly above the surface. This implies radiation into 4π steradians rather than 2π surface radiation or a compromise of 3π steradians (Bellot Rubio et al. 2000b).

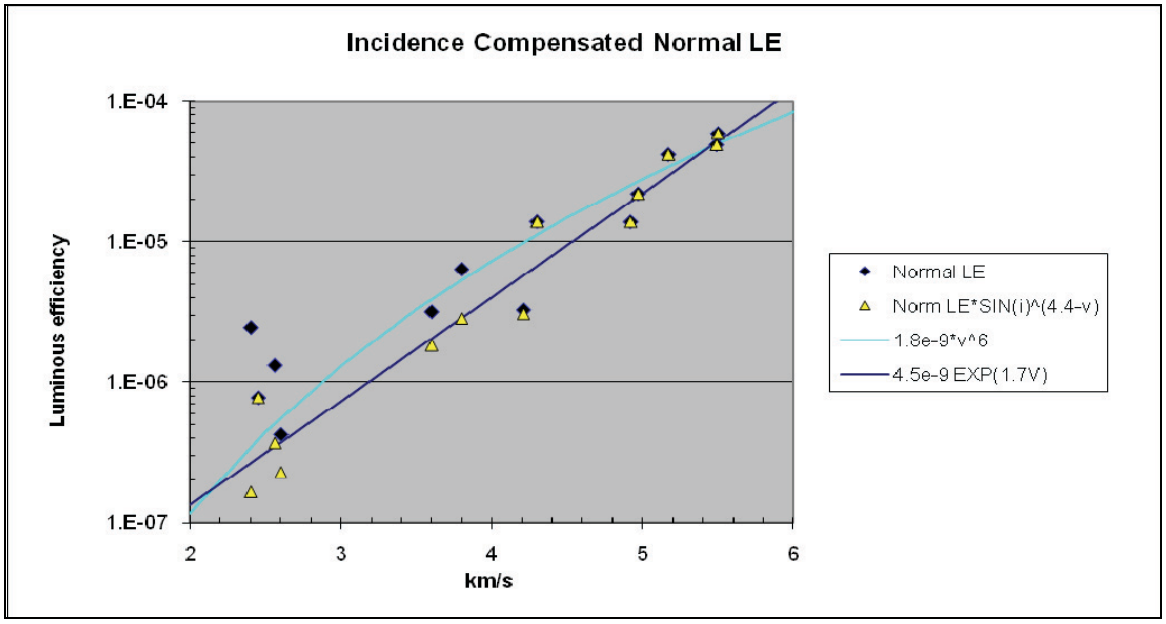

Figure 5. A trial fit compensating the luminous efficiency data for impact elevation was made for the vertical (normal) view. The normal, incidence compensated view is the one to use when comparing to meteoroid velocity lunar impacts.. Also shown is a power law velocity fits to V^6, light blue, and an exponential fit, dark line. The power law fit becomes absurd at meteoroid velocities giving $\eta > 1$ above 28.7 km/s.

Also shown in Figure 5 are trial fits to the incidence compensated η versus impact velocity data. As can be expected with a log-linear plot, a traditional power law fit appears curved while an exponential is a straight line fit to the data. The normal incidence data is approximated by a power law

fit of V^6 which, unfortunately, becomes improbable at meteoroid velocities giving $\eta > 1$ above 28.7 km/s. It is also difficult to imagine a physical model with such an exponent of velocity covering three orders of magnitude change for a less than 3x change in velocity. Simple exponential functions, although a better fit over the range of the data, also become unlikely at meteoroid velocities implying an exponential form that is not simply direct with velocity as is the one shown here. These questions drive much of the discussions to follow.

A luminous efficiency error analysis was performed for the η determinations yielding an estimated one sigma precision of 21% in η. The largest contributors to the error are the camera distance, the electron gain, the effective *QE* and the average energy per photon. The distance is problematic since the emission plume is a dynamic, three-dimensional object and each pixel views a part of the image at a different distance. Note that if one doubles this error the final uncertainty will increase by about 27% to 30%. The electron gain uncertainty, e-/IU, is relatively small but can be reduced further with careful spectral calibration. The effective *QE* and energy per photon uncertainties are both due to incomplete understanding of how the CCD reacts to the color changes in images of rapidly cooling particles. Refinements for future experiments are possible which would significantly reduce the uncertainty although, due to the extremely large dynamic range of the η data (up to five orders of magnitude), the estimated precision is deemed sufficient for current purposes.

4 Impact of Shock Waves in Materials

A logical first step to determine the correct scaling of impact luminous efficiency versus impact velocity is to briefly examine the internal energy produced by the initial impact shock wave itself and early post shock conditions. Indeed, this is the approach used in hydrocode modeling of impacts (Nemtchinov, 1998; Artemieva, 2000, 2001). One can then relate these conditions to the special case of the luminous efficiency of an impact into lunar regolith to deduce an appropriate model. One starts with a review of the basics (Melosh 1989; Lyzenga 1980).

Impact of a hypervelocity projectile with a solid target surface, such as that of a particle of regolith, produces shock waves which propagate from the point of impact through the target. The shock wave speed in the target, U_s can be represented by the linear Hugoniot shock velocity relation in the notation of Melosh (1989):

$$U_s = C_b + S\,u_p. \tag{4}$$

Here C_b is the bulk speed of sound in the target, u_p is the particle speed and S is an experimentally determined material property. Coupling at impact is determined by comparing the shock impedance Z_s of the target and the impactor:

$$Z_s \equiv \partial pressure / \partial velocity = \rho_0 U_s \tag{5}$$

$$\text{Then} \qquad P_s = Z_s u_p = \rho_0 U_s u_p \tag{6}$$

Here ρ_0 is the initial target density and P_s is the pressure behind the shock wave. Note that, from Equation 6 above, the shock pressure is second order in u_p, which in direct impact experiments is the impact velocity. A few idealized special cases serve to introduce the role of shock impedance. Assume the target and impactor are the same size and $Z_{target} < Z_{impactor}$ then the impactor and target move together

after impact at a reduced velocity. Similarly, if $Z_{target} > Z_{impactor}$ then the impactor bounces back from the target and target and impactor move in opposite directions. If both materials have the same shock impedance then the impactor will stop and the target will move away at the contact speed u_p. The extreme pressures P_s of the shock wave which give rise to acceleration of the target to u_p also give rise to irreversible effects which can include heating, thermal radiation, phase change, and decomposition. Due to the energy lost from the shock wave, U_s and thus u_p decline along the direction of propagation. This implies that, in a series of impacts, the energy transferred in each impact is some fraction of that of the preceding impact.

Early high pressure research (Walsh and Christian, 1955; McQueen et al., 1967) showed that solid materials under extreme pressure followed a pressure-volume curve characteristic of the material called the Hugoniot, Figure 6 (Lyzenga, 1980). Indeed, the determination of the Hugoniot for geophysical materials, (McQueen et al., 1967; Ahrens et al.,1969) is of central importance in planetary mantle investigations and drives much of the impact work to date. In a material which is transparent in the un-shocked state, shock temperature and shock velocity, V_s, can be measured by optical pyrometry. The work by Lyzenga (1980) and Lyzenga and Ahrens (1982) in which the primary thermal emissions from shocked transparent minerals are examined provides a useful introduction to the techniques involved. Shock emission techniques are further developed theoretically and experimentally by Svendsen et al. (1987) with attention paid to emissions from the shock interface. Of particular interest is the sensible (thermal) internal specific energy of the shocked state, which can be determined from the product of the change in volume times the change in pressure, $E' = \frac{1}{2}(V_0-V_1)\Delta P$, as in Figure 6, since this energy gives rise to the observed primary and secondary thermal emissions. Although similar determinations for opaque materials such as lunar regolith are not as easily performed the same principles apply. Also note that the physical properties of the material, including shock impedance, melting point, heat of fusion, emissivity, etc. all tend to vary along the Hugoniot adding an interesting complexity to the problem.

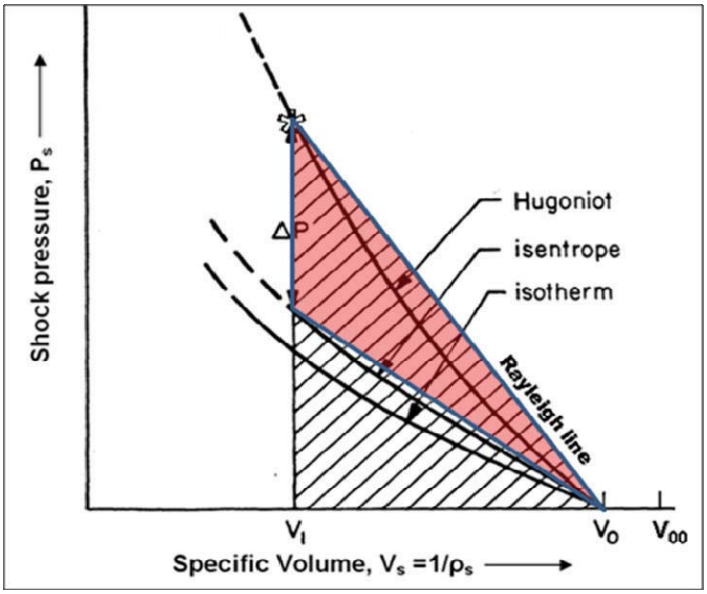

Figure 6. Simple Hugoniot compared with isotherm and isentrope of compression by Lyzenga (1980). Upon impact, a solid target is compressed along the Rayleigh line from V_o to V_1. Decompression after shock wave passage is at V_1 along ΔP followed by isentropic relaxation The total energy is given by the shaded area while the irreversible internal specific energy, the red portion, is $E' = \frac{1}{2}(V_0-V_1)\Delta P$.

The sensible portion of this internal energy is expressed immediately as a temperature change giving rise to the primary thermal radiation observed in transparent shocked materials. Although the shock temperature with phase change is less than it would be without phase change, observed shock temperature ranges from 4000 K to 8000 K as measured by multi channel optical pyrometry. A fast response (5 ns) is required since sample thicknesses of approximately 3 mm result in emissions lasting about a third of a microsecond while the shock wave traverses the material. Such direct emissions are consistent with the brief initial spike observed in impacts into pumice (Ernst and Schultz, 2007) and lunar simulant by a transparent projectile but not an opaque one. Investigations have been performed by Ahrens et al. (1973) and Ahrens and Cole (1974) using lunar regolith returned by the Apollo missions to determine their shock properties. Similar work (Anderson and Ahrens, 1998, Schmidt et al., 1994) has also been done for chondritic meteorites where the porosity was found to be of particular importance. After relaxation, the remaining sensible energy and much of the phase change internal energy will be found in thermal form providing the cooler but still hot particles observed in a laboratory or lunar impact into granular materials.

It is desirable to compare these investigations to the observations of higher velocity meteoroid impacts on the moon (Ahrens and O'Keef, 1972) and indeed the material properties determined in the laboratory are used in hydrocode simulations which attempt to answer similar questions. For current purposes, it is sufficient to note the following:

- Passage of shock wave leaves energy in the target
- This residual shock energy is expressed as heat in the target
- Residual specific energy (heat) is traditionally expressed as V^2
- Remainder of shock wave energy is passed on as kinetic energy
- Target material becomes an impactor with reduced kinetic energy
- Powder targets imply multiple serial impacts within the target

5 Shock Waves in Porous Materials and Powders

The moon is covered with a thick layer of porous lunar regolith so lunar impact emissions are governed in a large part by the porosity of the target. In the usual model, porous materials are first compacted to a dense state prior to the initiation of the shock wave into the body of the material. Although this compaction occurs at pressures well below that of the shock wave, volume changes and $\Delta P \Delta V$ work can be a significant contributor to the post shock temperature of the bulk material (Dijken and DeHosson, 1994a). For experiments to determine the Hugoniot of some material this "interface" heating is an annoying artifact but for impact sintering to form exotic materials the effect does useful work (Dijken and DeHosson, 1994b).

The approach taken by Dijken and De Hosson (1994a, 1994b) for powder sintering by impact is particularly instructive in that they couch the effects in term of impactor velocity u_p and the ratio of solid to powder specific volume V_0/V_{00}. In their approach, they follow a path in the P-V plane that compresses at zero pressure from initial powder specific volume V_{00} to solid density V_0 then compress with V_0 constant to the constant internal specific energy $(E'-E'_0)$ curve giving the shock pressure P_s as the starting point for determining u_s. This implies an additional internal energy component of $(V_{00}-V_0)P_S$. In their development, the powder is viewed as initially separated planes of identical solid material which, by symmetry, leads to the equipartition of internal and kinetic energy. One can define a

partition function B of energy in the target mass m_t between internal (thermal) and kinetic energy as follows:

$$KE_{impactor} = \tfrac{1}{2}\, m_i u_i^2 \geq (1-B) m_t (E' - E'_0) + B\ \mathrm{m_t u_t^2}/2 \qquad (7)$$

$$\text{Equipartition} \Rightarrow B = 1/2 \Rightarrow (E' - E'_0) = \tfrac{1}{2}\, \mathrm{u_t^2}$$

The simple equipartition approximation is shown to be particularly accurate (better than 5%) for loose powders with impactor velocities below 5 km/s when compared with data and more precise models (Dijken and DeHosson, 1994c). Lunar regolith (Ahrens and Cole 1974) with a bulk density of 1500 to 1800 kg/m^3 and a solid density averaging 3100 kg/m^3, has a relative powder density of 0.48 to 0.58, for which the above approximations are reasonable. The JSC-1a lunar regolith simulant (McKay et al. 1997) used in the above luminous efficiency determinations is by design very similar to the Apollo samples in these respects.

When one examines the internal energy effects of a sequence of impacts, Figure 7, each target particle becomes the impactor for the subsequent impact. From the equipartition assumption, *B = 1/2* and the energy is quickly expended in the powder as internal (thermal) energy within a short distance from the initial penetration track. One can imagine a similar result when the effect is generalized to a branched chain series of impacts. Radiation, conduction, and plasma quenching, all lead to a rapid statistical distribution of this energy within the initial zone. Although the primary impactor can have impedance significantly different from the solid particles of the powder giving an initial ratio, B_0, different from the equipartition assumption, the serial impacts between like particles in the regolith predominate. In any case, it is clear that the impactor energy is thermalized very rapidly in the penetration phase of the impact into regolith. This view is confirmed by recent high speed camera results by Ernst et al. (2010) which show that in the first 50 μs the energy of the impactor is primarily confined to several impactor radii of the impact. This compact thermal reservoir leads to a useful macroscopic thermal approach to the problem of energy partitioning in the impact zone.

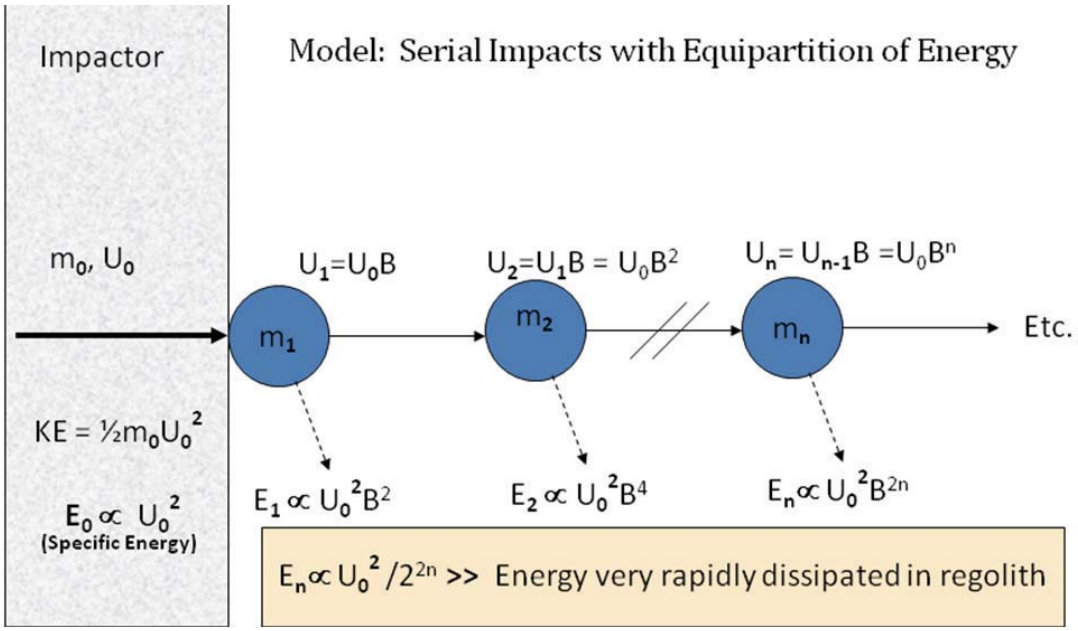

Figure 7. Cartoon of the effect of serial impacts in a particulate target. In the usual case, $B = \frac{1}{2}$ corresponding to equipartition of energy. Note that the specific kenetic energy expressed by velocity U_n declines extremely rapidly.

6 A Statistical Physics Approach

The impact zone defines a thermal reservoir of many small but macroscopic particles thermally linked with one another. These are precisely the assumptions used in the development of the canonical probability distribution of the particle energy states, Figure 8. It is a small extension of the canonical representation of the energy of particle r, E_r, in Joules to the representation of that energy as an energy density, E'_r in J/Mol. Similarly, the temperature parameter, $\beta = 1/kT$, becomes $1/RT$ when expressed as an energy density. The ratio remains unchanged. Similarly, the specific energy of particle r can be expressed as $E'_r = V^2_r$ in J/kg and the specific energy of the impact zone thermal system can be expressed as $E'_r = V^2_m$ in J/kg where V_m is the impactor velocity and V_r is the specific energy equivalent velocity of state r. The resulting probability of a particle being in state r becomes

$$P_r = Ce^{-V_r^2/V_m^2} \tag{8}$$

where C is the normalization constant. The energy density E'_T of any particular set of states, those states emitting visible radiation in this case, then becomes

$$E'_T = \sum_{r_{visible}} Ce^{-V_r^2/V_m^2}\Delta V_r^2 \tag{9}$$

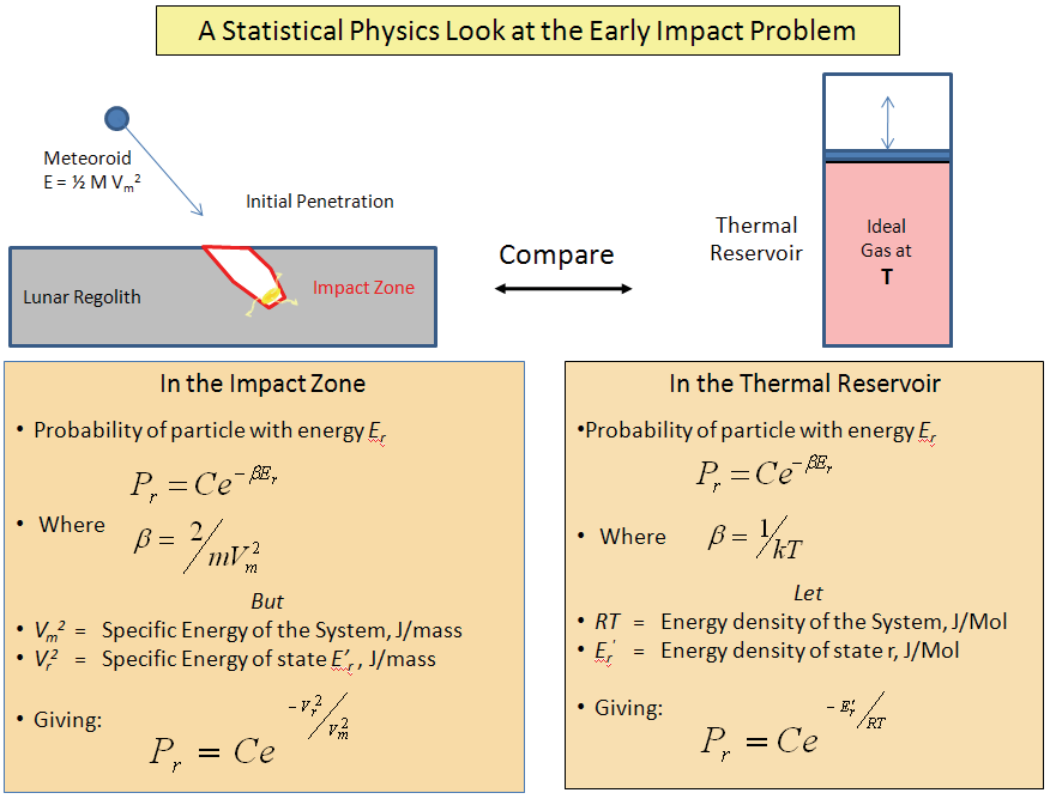

Figure 8. With hypervelocity impacts into particulate regolith, the impact specific energy is rapidly thermalised leading to a statistical physics approach. The specific energy of the impact is an exact analog of the canonical energy density of a thermal system leading to a canonical expression of the probability of a particle being in any particular energy state.

For the macro case of blackbody radiation the possible states, r, are numerous making V_r is essentially continuous allowing the summation in Equation 9 to be converted to an integral:

$$E'_T = C \int_{V_T^2}^{V_m^2} e^{-V_r^2 / V_m^2} d(V_r^2) \tag{10}$$

Where the energy densities are left as velocities squared for clarity. In Equation 10 the velocity of the lower limit, V_T is that of the lowest detectable energy. If the problem were to determine the portion of the energy expended to melt the regolith, then this would be just the square root of the minimum energy density of the molten material. For the cameras it would be the velocity equivalent of the coolest visible blackbody radiator. In Figure 9 the fraction of photons collected from a blackbody emitter are plotted versus temperature for a typical camera used for lunar impact studies. From this it becomes evident that there is no defined threshold, V_T ,for the lower limit which would enable the integral in Equation 10 to be evaluated directly. One can, however, somewhat arbitrarily put a lower bound on the visible blackbody temperature of 1000K for a ΔT of about 900K for these silicon Vis/NIR cameras. From this one can set a lower bound on V_T of about 1.2 km/s.

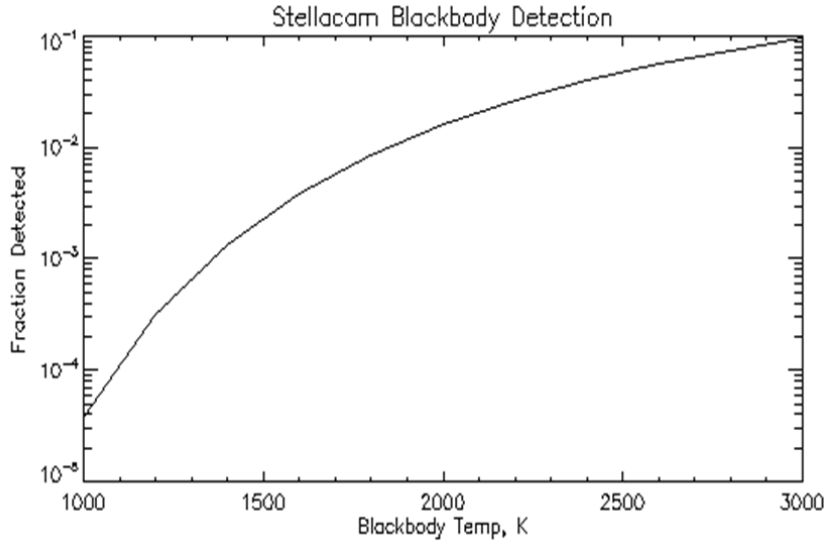

Figure 9. Fraction of blackbody emissions detected by the typical camera used for lunar impact flash detection. From this it is evident that there is no particular minimum detectable blackbody temperature. If 1000K is taken as a lower bound then the equivalent specific energy velocity, V_T would be about 1.2 km/s.

At this point we apply the Mean Value Theorem. When applied to Equation 10 the mean value theorem implies that:

there exists $V_C \in [V_T, V_m]$ such that $E'_T = C\left(V_m^2 - V_T^2\right) e^{-V_C^2 / V_m^2}$ (11)

IF $V_m^2 << V_T^2$ then $E'_T \cong C V_m^2 e^{-V_C^2 / V_m^2}$ (12)

Where an integration with a difficult limit, V_T , has been replaced with a characteristic velocity, V_c , and a simpler form in Equation 12. Note that for the usual case with an unresolved camera constant, O_c is lumped with the normalization constant, C. With E_T normalized as energy density E'_T and recognizing that $E'_m = V^2_m$ the luminous efficiency of the impact assumes a particularly simple form:

$$\text{since} \quad \eta = E_T / E_m = E'_T / V_m^2 \qquad \text{then} \quad \eta(V_m) = Ce^{-V_C^2 / V_m^2} \tag{13}$$

where one has two undetermined constants: a characteristic velocity V_C and a scaling factor C.

One can now use the luminous efficiencies determined from lunar impact observations in Table 1 with the light gas gun luminous efficiencies using the same cameras in Figure 5 to estimate the characteristic velocity V_C and scaling factor C. These results are shown in Figure 10, below. Also plotted for comparison are the historical luminous efficiency determinations of Bellot Rubio (2000) and Ernst and Schultz (2005). The data spans almost six orders of magnitude in η and ranges from just over 2 km/s to 71 km/s in velocity. Due to the form of Equation 13, it is immediately evident that the scaling factor is almost completely determined by the lunar impact data while the light gas gun data affects the critical velocity to a great extent. The lunar impact data yields a scaling factor estimate of $C = 1.5\times10^{-3}$ ± 10%. Due to the wide range and natural variability of the light gas gun data various fitting techniques gave slightly different results with characteristic velocity fit ranging from 9 km/s to almost 11 km/s. From this it is estimated that the critical velocity, V_c = 9.3 km/s ± 10%.

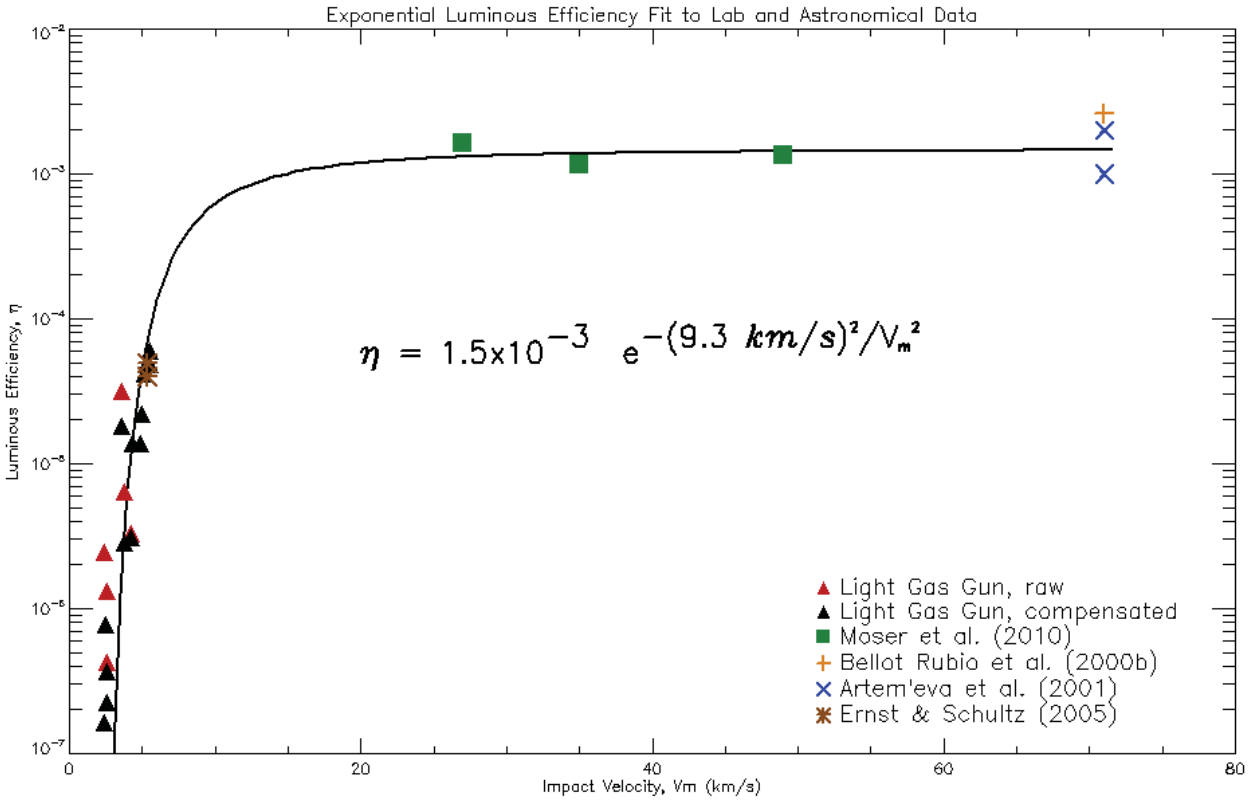

Figure 10. Lunar impact data from Table 1 is shown with light gas gun data from Figure 5 and historical data. The constants in Equation 13 are fit to the combined Table 1 and Figure 5 data. Characteristic velocity V_c is estimated to be 9.3 km/s and the scaling factor C is estimated to be 1.5×10^{-3}.

7 Conclusions

The luminous efficiency of hypervelocity impacts has been examined both in the laboratory and from observations of lunar meteoroid impacts. The luminous efficiency is a unique function of velocity with an extremely large variation with velocity in the laboratory range of 2 to 6 km/s, but a necessarily small variation with velocity in the meteoric range of 15 to 71 km/s. An exponential model of impact thermal emission efficiency is developed using fundamental principles of statistical physics which fits the combined laboratory and astronomical luminous efficiency data. This exponential model differs significantly from the polynomial models used to describe crater formation and dynamics. The model is valid for the early time portion of the process and focuses on the deposition of internal energy into the regolith which is subsequently observed as a bright blackbody flash. The model is compared with luminous efficiency data from laboratory impacts and from lunar impact observations. From these comparisons a critical velocity of 9.3 km/s and scaling factor of 1.5×10^{-3} are estimated. Further work to clarify the effects of mass and density of both the impactor and target upon the model is required. This model improves confidence in meteoroid mass estimates for lunar impacts and thus knowledge of the local space environment.

The unique energy partitioning approach embodied by luminous efficiency and this model can perhaps be extended to impact melting, another early time energy concern. Note that, since the melting point can be precisely known, Equation 10 can be evaluated directly. Although some melting is evident in light gas gun impacts into regolith it is not measurable while the light flash is. This is a possible starting point for future investigations.

Acknowledgements

Special thanks are due to the NASA Ames Vertical Gun Range crew for their efforts and to Dr. Peter Schultz of Brown University for help in coordinating those efforts. Work for this paper was supported in part by NASA contracts NNM05AB50C (Swift), NNM10AA03C (Moser) and the NASA Meteoroid Environments Office.

References

T. J. Ahrens, C. F. Petersen, and J. T. Rosenberg, Shock compression of feldspars, J. *Geophys. Res., 74*, 2727-2746 (1969)

T. J. Ahrens, and J. D. O'Keefe, Shock melting and vaporization of lunar rocks and minerals, *The Moon, 4*, 214-249 (1972)

T. J. Ahrens, J. D. O'Keefe, and R. V. Gibbons, Shock compression of a recrystallized anorthositic rock from Apollo 15, 4th Lunar Sci. Conf, Suppl. 4, *Geochim. Cosmochim. Acta, 3*, 2575-2590 (1973)

T. J. Ahrens, and D. M. Cole, Shock compression and adiabatic release of lunar fines from Apollo 17, Proc. 5th Lunar Science Conf., Suppl. 5, *Geochim. et Cosmochim. Acta, 3*, 2333-2345 (1974).

T. J. Ahrens, G. A. Lyzenga, and A. C. Mitchell, Temperatures induced by shock waves in minerals, In *High pressure research in geophysics,* edited by S. Akimoto and M.H. Manghnani, pp 579–594, Center for Academic Publications, Japan (1982).

W. W. Anderson, and T. J. Ahrens, Shock wave equations of state of chondritic meteorites, in *Shock Compression of Condensed Matter - 1997*, edited by S. C. Schmidt, et al., pp. 115-118, AIP Press, Woodbury, NY, 1998 (1997).

O. L. Anderson, and R. C. Liebermann, Sound velocities in rocks and Minerals, VESIAC State-of-the-Art Report 7885-4-X, *Inst. Sci. Techn.,* Univ. Michigan, Ann Arbor(1966).

N.A. Artemieva, V.V. Shuvalov, I.A. Trubetskaya, Lunar Leonid Meteors- Numerical Simulations, *Lunar and Planetary Science Conference XXXI*, paper 1402 (2000).

N.A. Artemieva, I.B. Kosarev, I.V. Nemtchinov, I.A. Trubetskaya, and V.V. Shuvalov, *SoSyR* **35**(3), 177-180 (2001a).

L. R. Bellot Rubio, J. L. Ortiz, and P. V. Sada, Observation And Interpretation Of Meteoroid Impact Flashes On The Moon, *Earth, Moon, and Planets, v. 82/83*, p. 575-598 (2000a).
L. R. Bellot Rubio, J. L. Ortiz, and P. V. Sada, Luminous Efficiency in Hypervelocity Impacts from the 1999 Lunar Leonids, *The Astrophysical Journal, 542*:L65-L68 (2000b).
M. B. Boslough, and T. J. Ahrens, Particle Velocity Experiments in Anorthosite and Gabbro, in *Shock Waves in Condensed Matter-1983*, edited by J. R. Asay *et.al.,* Elsevier Science Publishers (1984).
W. J. Cooke, R.M. Suggs, and W.R. Swift, A Probable Taurid Impact on the Moon, *Lunar and Planetary Science Conference XXXVII*, paper 1731 (2006).
W. J. Cooke, R.M. Suggs, W.R. Swift, and N.P. Hollon, Rate And Distribution Of Kilogram Lunar Impactors, *Lunar and Planetary Science Conference XXXVIII*, Paper 1986 (2007).
B. M. Cudnik, D. W. Dunham, D. M. Palmer, A. C. Cook, R. J. Venable, and P. S. Gural Ground-Based Observations of High Velocity Impacts on the Moon's Surface – The Lunar Leonid Phenomena of 1999 and 2001, *Lunar and Planetary Science Conference XXXIII*, Paper 1329 (2002).
B. M. Cudnick, D. W. Dunham, D. M. Palmer, A. C. Cook, R. J. Venable, and P. S. Gural The Observation and Characterization of Lunar Meteroid Impact Phenomena, *Earth, Moon and Planets 93***:** 97–106 (2003).
D. K. Dijken, and J. Th. M. De Hosson Thermodynamic Model of the Compaction of Powder Materials by Shock Waves, *J. Appl. Phys. 75 (1)*, p.203 (1994a).
D. K. Dijken, and J. Th. M. De Hosson , Shock Wave Equation of State of Powder Material, *J. Appl. Phys. 75 (2)*, p 809 (1994b).
D. K. Dijken, and J. Th. M. De Hosson Shock Wave Velocity and Shock Pressure for low density powders: A Novel Approach, *Appl. Phys. Lett. 64 (7)*, p. 933 (1994c).
D.W. Dunham, B. Cudnick, D.M. Palmer, P.V. Sada, H.J. Melosh, M. Beech, R. Frankenberger, L. Pellerin, R. Venable, D. Asher, R. Sterner, B. Gotwols, B. Wun, and D. Stockbauer, *LPSC XXXI*, Paper 1547 (2000).
C. M. Ernst, and P. H. Schultz, Early Time Temperature Evolution of the Impact Flash and Beyond, *Lunar and Planetary Science Conference XXXV*, Paper 1986 (2004).
C. M. Ernst, and P. H. Schultz, Investigations of the Luminous energy and Luminous Efficiency of Experimental Impacts into Particulate Targets, *Lunar and Planetary Science Conference XXXVI*, paper 1475 (2005).
C. M. Ernst, and P. H. Schultz, Temporal and Spatial Resolution of the Early-Time Impact Flash: Implications for Light Source Distribution, *Lunar and Planetary Science Conference XXXVIII*, paper 2353 (2007).
C. M. Ernst, O. S. Barnouin, and P. H. Schultz, *Lunar and Planetary Science Conference XLI*, paper 1381 (2010).
D. E. Gault, E. D. Heitowit, and H. J. Moore Some Observations of Hypervelocity Impacts with Porous Media, *Proceedings of the Lunar Surface Materials Conference*, Academic Press, Boston, Massachusetts, 1964 (1963).
G. Heiken, D. Vaniman and B. French, *Lunar Sourcebook - A Users Guide to the Moon*. Cambridge University Press, Cambridge, UK (1991).
K. A. Holsapple and R. M. Schmidt, Point Source Solutions and Coupling Parameters in Cratering Mechanics, *J. Geophys. Res., 92*, *No. B7*, p. 6350 (1987).
K. A. Holsapple, The Scaling of Impact Processes in Planetary Sciences, *Ann Rev. Earth Planet. Sci, 21,* p. 333-373 (1993).
R. C. Liebermann and A. E. Ringwood, Elastic properties of anorthite and the nature of the lunar crust, *Earth Planet. Sci. Letters, 31*, 69-74 (1976).
G. A. Lyzenga, Shock Temperatures of Materials: Experiments and Applications to the High-Pressure Equation of State, Ph.D. dissertation, California Institute of Technology, Pasadena, California (1980).
D. S. McKay, J.L. Carter, W.W. Boles, C.C. Allen and J.H. Allton, JSC-1: A new Lunar Regolith Simu1lant, *Lunar and Planetary Science Conference XXIV*, 963 (1997).
R. C. McQueen, S. P. Marsh and J. N. Fritz, Hugoinoit equations of state of twelve rocks, *J. Geophys. Res., 72*, 4999-5036 (1967).
H. J. Melosh, *Impact Cratering, a Geological Process,* Oxford University Press, New York (1989)
H. J. Melosh, N. A. Artemieva, A. P. Golub, I. V. Nemchinov, V.V. Shuvalov, and I. A. Trubetskaya, Remote Visual Detection of Impacts on the Lunar Surface, *Lunar and Planetary Science Conference XXIV*, 975 (1993).
D. E. Moser, R.M. Suggs, W. R. Swift, R. J. Suggs, W. J. Cooke, A. M. Diekmann, H. M. Koehler, *Meteoroids 2010*, Breckenridge, CO (2010).
I.V. Nemtchinov, V. V. Shuvalov, N. A. Artemieva, B. A. Ivanov, I. B. Kosarev, and I. A. Trubetskaya, Light Impulse Created by Meteoroids Impacting the Moon, *Lunar and Planetary Science Conference XXIX*, 1032 (1998).
J.L. Ortiz, P.V. Sada, L.R. Bellot Rubio, F.J. Aceituno, J. Aceituno, P.J. Gutiérrez, and U. Thiele, *Nature* **405**, 921-923 (2000).
J.L Ortiz, J.A. Quesada, J. Aceituno, F.J. Aceituno, and L.R. Bellot Rubio, *ApJ* **576**, 567-573 (2002).

J. L. Ortiz, F. J. Aceituno, J. A. Quesada, J. Aceituno, M. Fernández, P. Santos-Sanz, J. M. Trigo-Rodríguez, J. Llorca, F. J. Martín-Torres, P. Montañés-Rodríguez, and E. Pallé, Detection of Sporadic Impact Flashes on the Moon: Implications for the Luminous Efficiency of Hypervelocity Impacts and Derived Terrestrial Impact Rates. *Icarus 184*, 319-326. (2006).

R. T. Schmitt, A. Deutsch, and D. Stöffler, Calculation of Hugoniot Curves and Post-Shock Temperatures for H- and L-Chondrites, *Lunar and Planetary Science Conference XXV*, p.1209 (1994).

R. M. Suggs, W. Cooke, R. J. Suggs, H. McNamara, W. Swift, D. Moser, and A. Diekmann, Flux of Kilogram-sized Meteoroids from Lunar Impact Monitoring., *Bulletin of the American Astronomical Society 40*, 455 (2008a).

R. M. Suggs, W. J. Cooke, R. J. Suggs, W. R. Swift, and N. Hollon, The NASA Lunar Impact Monitoring Program, *Earth, Moon, and Planets 102*, 293 (2008b).

R.M. Suggs, W.J. Cooke, H.M. Koehler, D.E. Moser, R.J. Suggs, and W.R. Swift, *Meteoroids 2010*, Breckenridge, CO (2010).

B. Svendsen, T. J. Ahrens, and J. D. Bass, Optical radiation from shock-compressed materials and interfaces, *High Pressure Research in Mineral Physics*, edited by M. Manghnani and Y. Syono, pp. 403-426, Terra Scientific Publishing Co., Tokyo (1987).

D. C. Swift, A. Seifter, D. B. Holtkamp, V. W. Yuan, D. Bowman, and D. A. Clark, Explanation of anomalous shock temperatures in shock-loaded Mo samples measured using neutron resonance spectroscopy,*Phys. Rev. B, vol. 77,* 092102 (2008).

W.R. Swift, R.M. Suggs, and W.J. Cooke, *Earth Moon Planets* **102**, 299-303 (2008).

Swift, W., Suggs, R., and Cooke, B. 2008. Algorithms for Lunar Flash Video Search, Measurement, and Archiving. *Earth, Moon, and Planets* **102**, 299.

J. M. Walsh and R. H. Christian, Equation of state of metals from shock wave measurements, *Phys. Rev., 97*, 1544-1556 (1955).

M. Yanagisawa and N. Kisaichi, Lightcurves of 1999 Leonid Impact Flashes on the Moon, *Icarus* **159**, 31–38 (2002).

M. Yanagisawa, K. Ohnishi, Y. Takamura, H. Masuda, Y. Sakai, M. Ida, M. Adachi, and M. Ishida, *Icarus* **182**(2), 489-495 (2006).

M. Yanagisawa, H. Ikegami, M. Ishida, H. Karasaki, J. Takahashi, K. Kinoshita, and K. Ohnishi, *M&PSA* **43**, Paper 5169 (2008).

X. Zeng,, C. He, H. A. Oravec, A. Wilkinson, J. H. Agui, and V. M. Asnani,. Geotechnical Properties of JSC-1A Lunar Soil Simulant. Journal of Aerospace Engineering 23, no. 2: 111 (2010).